A Section 508–conformant HTML version of this article is available at https://doi.org/10.1289/EHP4709.

Exposure to Air Pollution during Pregnancy and Childhood, and White Matter Microstructure in Preadolescents

Małgorzata J. Lubczyńska,[1,2,3] Ryan L. Muetzel,[4,5] Hanan El Marroun,[4,6,7] Xavier Basagaña,[1,2,3] Maciej Strak,[8] William Denault,[9,10,11] Vincent W.V. Jaddoe,[5,7] Manon Hillegers,[4] Meike W. Vernooij,[12,13] Gerard Hoek,[8] Tonya White,[4,13] Bert Brunekreef,[8,14] Henning Tiemeier,[4,15] and Mònica Guxens[1,2,3,4]*

[1]Barcelona Institute for Global Health (ISGlobal)–Campus Mar, Barcelona, Spain
[2]Pompeu Fabra University, Barcelona, Spain
[3]Spanish Consortium for Research on Epidemiology and Public Health (CIBERESP), Instituto de Salud Carlos III, Madrid, Spain
[4]Department of Child and Adolescent Psychiatry/Psychology, Erasmus University Medical Centre–Sophia Children's Hospital, Rotterdam, Netherlands
[5]The Generation R Study Group, Erasmus University Medical Centre, Rotterdam, Netherlands
[6]Department of Psychology, Education and Child Studies, Erasmus School of Social and Behavioural Sciences, Rotterdam, Netherlands
[7]Department of Pediatrics, Erasmus University Medical Centre–Sophia Children's Hospital, Rotterdam, Netherlands
[8]Institute for Risk Assessment Sciences, Utrecht University, Utrecht, Netherlands
[9]Department of Genetics and Bioinformatics, Norwegian Institute of Public Health, Oslo, Norway
[10]Department of Gobal Public Health and Primary Care, University of Bergen, Bergen, Norway
[11]Center for Fertility and Health (CeFH), Norwegian Institute of Public Health, Oslo, Norway
[12]Department of Epidemiology, Erasmus University Medical Centre, Rotterdam, Netherlands
[13]Department of Radiology and Nuclear Medicine, Erasmus University Medical Centre, Rotterdam, Netherlands
[14]Julius Center for Health Sciences and Primary Care, University Medical Center Utrecht, Utrecht, Netherlands
[15]Department of Social and Behavioral Science, Harvard T.H. Chan School of Public Health, Boston, Massachusetts, USA

Background: Air pollution has been related to brain structural alterations, but a relationship with white matter microstructure is unclear.

Objectives: We assessed whether pregnancy and childhood exposures to air pollution are related to white matter microstructure in preadolescents.

Methods: We used data of 2,954 children from the Generation R Study, a population-based birth cohort from Rotterdam, Netherlands (2002–2006). Concentrations of 17 air pollutants including nitrogen oxides (NO_X), particulate matter (PM), and components of PM were estimated at participants' homes during pregnancy and childhood using land-use regression models. Diffusion tensor images were obtained at child's 9–12 years of age, and fractional anisotropy (FA) and mean diffusivity (MD) were computed. We performed linear regressions adjusting for socioeconomic and lifestyle characteristics. Single-pollutant analyses were followed by multipollutant analyses using the Deletion/Substitution/Addition (DSA) algorithm.

Results: In the single-pollutant analyses, higher concentrations of several air pollutants during pregnancy or childhood were associated with significantly lower FA or higher MD ($p < 0.05$). In multipollutant models of pregnancy exposures selected by DSA, higher concentration of fine particles was associated with significantly lower FA [−0.71 (95% CI: −1.26, −0.16) per 5 $\mu g/m^3$ fine particles] and higher concentration of elemental silicon with significantly higher MD [0.06 (95% CI: 0.01, 0.11) per 100 ng/m^3 silicon]. Multipollutant models of childhood exposures selected by DSA indicated significant associations of NO_X with FA [−0.14 (95% CI: −0.23, −0.04) per 20-$\mu g/m^3$ NO_X increase], and of elemental zinc and the oxidative potential of PM with MD [0.03 (95% CI: 0.01, 0.04) per 10-ng/m^3 zinc increase and 0.07 (95% CI: 0.00, 0.44) per 1-nmol DTT/min/m^3 oxidative potential increase]. Mutually adjusted models of significant exposures during pregnancy and childhood indicated significant associations of silicon during pregnancy, and zinc during childhood, with MD.

Discussion: Exposure in pregnancy and childhood to air pollutants from tailpipe and non-tailpipe emissions were associated with lower FA and higher MD in white matter of preadolescents. https://doi.org/10.1289/EHP4709

Introduction

The evidence for the harmful effects of air pollution on human health is increasing (Beelen et al. 2014; Chen et al. 2017; Kaufman et al. 2016; Pedersen et al. 2013; Raaschou-Nielsen et al. 2013). Animal studies focusing on the association between exposure to air pollution and brain health are leading to growing documentation of a relationship with neuroinflammation and oxidative stress (Block et al. 2012). Due to the relatively immature detoxification mechanisms of fetuses and infants as well as the many developmental processes taking place during pregnancy and childhood, direct and indirect exposures to air pollution during these developmental periods could lead to alterations in the brain even at relatively low levels of exposure (Block et al. 2012; Grandjean and Landrigan 2014).

To date, most epidemiological studies have used neuropsychological instruments to assess the relationship between exposure to air pollution and child's neurodevelopment, demonstrating relationships between higher exposures and lower cognitive performance, impaired motor function, and more behavioral problems (Suades-González et al. 2015). However, these studies provide limited understanding of potential structural and functional brain alterations that underlie these associations. The use of magnetic resonance imaging (MRI) allows for the identification of such alterations, and the limited number of existing studies using MRI have found evidence for associations between exposure to air pollution during pregnancy or childhood and white and gray matter abnormalities, generally indicating a decrease in white and gray matter mass with higher exposure to air pollution (Calderón-Garcidueñas et al. 2008, 2011; Guxens et al. 2018; Mortamais et al. 2017; Peterson et al. 2015; Pujol et al. 2016a, 2016b). To our knowledge, the use of diffusion tensor imaging to quantify white matter microstructure in relation to air pollution exposures has been limited to a single study that showed that airborne elemental copper was associated with

Address correspondence to Mònica Guxens, Barcelona Institute for Global Health–Campus Mar, Doctor Aiguader 88, 08003 Barcelona. Telephone: 34 932 147 330. Email: monica.guxens@isglobal.org

Supplemental Material is available online (https://doi.org/10.1289/EHP4709).

*Current address: National Institute of Public Health and the Environment (RIVM), Bilthoven, Netherlands.

The authors declare they have no actual or potential competing financial interests.

Received 7 November 2018; Revised 7 January 2020; Accepted 17 January 2020; Published 13 February 2020.

Note to readers with disabilities: *EHP* strives to ensure that all journal content is accessible to all readers. However, some figures and Supplemental Material published in *EHP* articles may not conform to 508 standards due to the complexity of the information being presented. If you need assistance accessing journal content, please contact ehponline@niehs.nih.gov. Our staff will work with you to assess and meet your accessibility needs within 3 working days.

differences in white matter microstructure adjacent to the caudate nucleus (Pujol et al. 2016b). Unlike anatomical imaging, which is used to measure the white and gray matter structure of the brain, diffusion tensor imaging measures the magnitude and the directionality of water diffusion within the white matter. These microstructural properties measured by diffusion tensor imaging allow detection of subtle alterations in white matter that may not be observable with conventional anatomical imaging and which may reveal characteristics typifying healthy brain development (Schmithorst and Yuan 2010) as well as characteristics that could be indicative of various psychiatric disorders (White et al. 2008). The diffusion profile of white matter can be expressed with the use of two common scalar values: fractional anisotropy (FA), which indicates the overall directionality of water diffusion, and mean diffusivity (MD), which describes the magnitude of water diffusion within brain tissue. One of the most important processes for optimal brain development is myelination, which is essential for efficient functioning of the brain through quick and healthy neural communication (van Tilborg et al. 2018). Myelination starts, on average, 28 weeks after conception and continues throughout adolescence and is responsible for increases in relative white matter volume and for water diffusion changes within white matter tracts (van Tilborg et al. 2018), which can be examined using diffusion tensor imaging. Moreover, diffusion tensor images reveal information about the density of axonal fiber packing in the brain, another measure that is indicative of white matter integrity (Dimond et al. 2019).

Existing studies on the relationship between exposure to air pollution and neurodevelopment assessed using MRI have analyzed a relatively narrow number of air pollutants, thereby limiting the opportunity to disentangle which pollutants are most harmful. This becomes relevant when different pollutants reflect different sources of exposure, such as tailpipe emissions, brake linings, or tire wear markers. In addition, to our knowledge, the existing studies have focused on exposure during either pregnancy or childhood, but not both. Given that myelination is a process that occurs across both these developmental periods (van Tilborg et al. 2018), understanding whether the timing of exposure to air pollution has a distinct and negative impact on neurodevelopment is crucial. Moreover, regarding exposure assessment during childhood, the existing studies that analyzed the relationship between childhood exposures and neurodevelopment assessed using MRI looked at either exposures measured using urinary metabolites or exposures measured at schools, which likely reflect different sources of pollution and/or different exposure conditions. Therefore, we aimed to analyze the associations between pregnancy and childhood residential exposures to a wide range of air pollutants with white matter microstructure in preadolescents. Our hypothesis was that higher exposure to air pollution is associated with lower FA and higher MD of white matter, generally associated with impaired neurodevelopment.

Methods

Population and Study Design

This study is embedded in the Generation R Study, a study of a population-based birth cohort from pregnancy onward, based in the urban area of Rotterdam, Netherlands (Kooijman et al. 2016). A total of 8,879 women were enrolled during pregnancy and an additional 899 women were recruited shortly after delivery. The children were born between April 2002 and January 2006, and we included only singleton pregnancies in our study, resulting in 9,610 children. When the children were between 9 and 12 years of age, those still involved in the study were invited to participate in an MRI session ($n = 8{,}548$) (White et al. 2018). In total, 3,992 mothers and their children complied with the invite and consented in writing (White et al. 2018). From this total, 2,954 children had good quality imaging scans and data on air pollution and were included in this analysis. The Medical Ethics Committee of the Erasmus Medical Centre in Rotterdam, Netherlands, granted ethical approval for the study.

Exposure to Air Pollution

Air pollution concentrations were estimated for all reported home addresses of each participant during the pregnancy and childhood following a standardized procedure (Guxens et al. 2018; de Hoogh et al. 2013; Jedynska et al. 2014; Montagne et al. 2015; Yang et al. 2015). In brief, within the European Study of Cohorts for Air Pollution Effects (ESCAPE) and Transport related Air Pollution and Health impacts–Integrated Methodologies for Assessing Particulate Matter (TRANSPHORM) projects, three 2-week measurements of nitrogen dioxide (NO_2) and nitrogen oxides (NO_X) were performed in the warm, cold, and intermediate seasons between February 2009 and February 2010 at 80 sites spread across the Netherlands and Belgium (Montagne et al. 2015). In addition, at 40 of those sites particulate matter (PM) with aerodynamic diameter <10 μm (PM_{10}), between 10 μm and 2.5 μm (PM_{coarse}), <2.5 μm ($PM_{2.5}$), absorbance of $PM_{2.5}$ fraction ($PM_{2.5}$ absorbance), and composition of $PM_{2.5}$ consisting of polycyclic aromatic hydrocarbons (PAHs), benzo[a]pyrene (B[a]P), organic carbon (OC), copper (Cu), iron (Fe), potassium (K), silicon (Si), zinc (Zn), and the oxidative potential of $PM_{2.5}$ (OP) measurements were carried out (de Hoogh et al. 2013; Jedynska et al. 2014; Yang et al. 2015). The OP was evaluated using two acellular methods: dithiothreitol (OP_{DTT}) and electron spin resonance (OP_{ESR}) (Yang et al. 2015). Another campaign within the MUSiC (Measurements of Ultrafine particles and Soot in Cities) project measuring PM with aerodynamic diameter <0.1 μm [ultrafine particles (UFPs)] was held in 2013 at 80 sites in Rotterdam (Montagne et al. 2015). The number concentrations of UFPs were measured in real time for 30 min at each site in three different seasons. For each pollutant, the results of the measurements were averaged, adjusting for temporal trends using data from a continuous reference site, resulting in one annual mean concentration for each pollutant.

A variety of potential land use predictors, such as proximity to the nearest road, traffic intensity on the nearest road, and population density, was then assigned to each monitoring site, and linear regression modeling was applied to determine which combination of predictors explained the concentrations of the pollutants most accurately, resulting in land-use regression (LUR) models (de Hoogh et al. 2013; Jedynska et al. 2014; Montagne et al. 2015; Yang et al. 2015). In this study, we focused only on pollutants whose LUR models included at least one traffic predictor. Next, these LUR models were applied to each address that the participants had lived at during the period of interest, that is, since conception until the MRI session. Taking into account the time spent at each address and weighting the pollution concentrations accordingly, we then obtained a single mean air pollution concentration of each pollutant for each participant for the pregnancy period (i.e., since conception until birth) and for the childhood period (i.e., since birth until the MRI session). From the 899 participants who were recruited shortly after birth, 310 were included in this analysis, and we considered their address at birth as representative for the pregnancy period. Because no historical data was available for the majority of the pollutants under study to perform back- and forward extrapolation of the concentrations to match the exact periods of interest, we assumed that the spatial contrast remained constant over time as has been previously demonstrated in the Netherlands for a period of up to 8 y (1999–2007) (Eeftens et al. 2011) and in Great Britain for a period of up to 18 y (1991–2009) (Gulliver et al. 2013).

Diffusion Tensor Imaging

Image acquisition. To familiarize participants with the magnetic resonance environment and therefore reduce the possibility of failure to complete the scanning session, each child underwent a half-hour mock scanning session prior to the actual MRI (White et al. 2018). To limit the movement of the head, the participating children were accommodated by providing them with a thorough explanation before the scanning session, the possibility to watch a movie or listen to music during the session, and by placement of cushions around the head to fixate the head in a comfortable way. The scans were performed on a 3 Tesla General Electric scanner (MR750W; GE) using an 8-channel receive-only head coil. Diffusion tensor imaging data were obtained using an axial spin echo with 35-direction echo planar imaging sequence [repetition time (TR) = 12.500 ms, echo time (TE) = 72 ms, field of view = 240 mm × 240 mm, acquisition matrix = 120 × 120, slice thickness = 2 mm, number of slices = 65, asset acceleration factor = 2, b = 900 s/mm^2].

Image preprocessing. The image preprocessing was performed with the use of the FMRIB Software Library (FSL), version 5.0.9 (Jenkinson et al. 2012). First, the images were modified to exclude nonbrain tissue and then rectified for artifacts induced by eddy currents and for translations or rotations that potentially arose due to minor movement of the head during the scanning session. The B-table was then rotated based on the rotations calculated and applied to the diffusion data during the eddy–current correction step. Next, using the RESTORE approach from the Camino diffusion MRI toolkit (Cook et al. 2006), a diffusion tensor was fitted at each voxel, followed by the computation of FA and MD.

Probabilistic tractography. To establish connectivity distributions for several large fiber bundles, the automated FSL plugin AutoPtx (de Groot et al. 2015) was used to perform probabilistic white matter fiber tractography on the scans of each participant. This package includes a set of predefined seed, target, and exclusion masks for a number of large white matter tracts. After a nonlinear registration of the FA map of each participant to the FMRIB58 FA map, these predefined seed, target, and exclusion masks were warped back to each participant's native space. The FSL Bayesian Estimation of Diffusion Parameters Obtained Using Sampling Techniques (BEDPOSTx) along with the FSL ProbtrackX were used, taking into account two fiber orientations, to conduct probabilistic fiber tractography (Behrens et al. 2003, 2007). The amount of successful seed-to-target attempts from the identified connectivity distributions were used to normalize the connectivity distributions, followed by introduction of a threshold to eliminate voxels that were implausible to belong to the true distribution. By weighting voxels based on the connectivity distribution, with voxels with higher probability of being part of the true distribution receiving higher weight, average FA and MD values were assessed for each white matter tract.

DTI quality assurance. For automatic assessment of slice-wise variation and properties of artifacts in each diffusion-weighted volume, the DTIPrep tool (https://www.nitrc.org/projects/dtiprep/) was used. Next, maps of sum-of-squares error (SSE) from the calculations of diffusion tensor were studied for signals characteristic of artifacts. Each SSE map was classified by a value from 0 to 3, with 0 indicating no artifacts, 1 indicating mild artifacts, 2 indicating moderate artifacts, and 3 indicating severe artifacts. If the automated quality control or the SSE map inspection was poor, indicating a substantial presence of artifacts, these cases were excluded from analyses. This was denoted by a structured-pattern high signal intensity in the SSE map on one or more slices, not including, for example, the ventricles or nonbrain tissue. Examples include substantial ghosting artifacts, entire slices with high signal intensity (indicative of substantial motion). Ratings of 1 or 2 (mild and moderate artifacts, respectively) was rated when data contained no more than three slices with mildly increased structured signal (i.e., not high/strong, not in ventricles/nonbrain areas) in the SSE map. SSE maps were rated independently of the automated DTIPrep results (and vice versa), and thus data could be excluded due to failing any of the checks done (i.e., some data sets were excluded for only SSE issues, only DTIPrep issues, only registration issues, or some combination of issues). Finally, an examination of accuracy with respect to the nonlinear registration of the scans to standard space was performed to ensure seed and target masks for tractography were properly aligned to native space. Nonlinear registration was checked by building a four-dimensional nifti file containing all subjects' co-registered FA maps, such that the fourth dimension was subject. Images were visually inspected one at a time for major deviations from the template, either in rotations, translations, or over-warping in certain areas (more than ∼2 voxels of shift from the template). Proper whole-brain coverage was also inspected during this step, and some subjects missing substantial portions of the brain (leading to over-warping of the nonlinear registration) were also flagged.

Construction of global DTI metrics. In order to estimate a global estimate of FA and MD, which may better capture associations that have relatively small effect sizes that spatially are widespread in the brain, we ran a confirmatory factor analysis on scalar metrics from 12 commonly defined white matter tracts: cingulum bundle, corticospinal tract, inferior longitudinal fasciculus, superior longitudinal fasciculus, uncinate fasciculus (one per hemisphere), forceps minor and forceps major (interhemispheric). The confirmatory factor analysis essentially generates a weighted average of all 12 tracts based on the factor loadings. For FA and MD, a separate (although identically structured) factor analysis was run to produce a factor score (a global metric of FA and MD) (Muetzel et al. 2018). Global metrics are factors scores from a confirmatory factor analysis (i.e., standardized scores centered on 0 and ranging from roughly −5 to 5 for FA, and −0.5 to 0.5 for MD) and thus do not conform to the standard values typically seen with DTI (e.g., FA ranging from 0 to 1). All FA values from specific tracts are presented on the proper scale (e.g., for FA from 0 to 1). For the MD values from specific tracts, a scaling factor of 10^9 was used. FA indicates the tendency for preferential water diffusion in white matter tracts, which is lower in white matter with certain features (e.g., white matter tracts in which the comprising axons are less densely packed and the directionality of the water diffusion is not uniformly directed as compared with well-organized tracts). MD describes the magnitude of average water diffusion in all directions within brain tissue, with higher values generally occurring in white matter tracts that show a less well-organized structure.

Potential Confounding Variables

Potential confounding variables included in the models were selected based on scientific literature and on availability of data within the Generation R cohort (Guxens et al. 2018). Maternal and paternal educational level (primary education or lower/secondary education/higher education), monthly household income (<900€/900€–1,600€/1,600€–2,200€/ > 2,200€), maternal and paternal country of birth (the Netherlands/other Western/non-Western), maternal and paternal age at enrollment in the cohort (continuous in years), maternal smoking during pregnancy (never/smoking use until pregnancy known/continued smoking during pregnancy), maternal alcohol consumption during pregnancy (never/alcohol use until pregnancy known/continued alcohol use during pregnancy), parity (nulliparous/one child/two or more children), marital status (married/living together/no partner), and maternal and paternal psychological distress (continuous) using the Brief Symptom Inventory (De Beurs 2004) were collected by questionnaires during pregnancy. Maternal and paternal weight and height (continuous in kilograms and centimeters, respectively) were measured or self-reported in the first trimester of pregnancy,

and maternal and paternal body mass index (BMI) was calculated based on the collected weight and height data. Maternal and paternal height were included in the models as potential confounding variables separately from BMI because they could be associated with the outcome variables independent from BMI. Maternal intelligence quotient (continuous) was assessed at child's age of 6 y with Ravens Advanced Progressive Matrices Test, set I (Raven 1962). Using multidimensional scaling, child's genetic ancestry was estimated based on the genome-wide single-nucleotide polymorphism data from whole blood at birth, and four principal components of ancestry (continuous) were included here to better correct for population stratification (Neumann et al. 2017; Price et al. 2006). Child's sex (boy/girl) was obtained from hospital records at birth and child's age (continuous in years) was collected at the scanning session.

Statistical Analyses

We first applied multiple imputation of missing values using chained equations to impute missing potential confounding variables among all participants with available data on the exposure and the outcome. We obtained 25 completed data sets, which we analyzed using standard procedures for multiple imputation (see Table S1). Children included in the analysis ($n = 2{,}954$) were more likely to have parents from a higher socioeconomic position compared with children who were not included ($n = 6{,}656$) (Table 1). To correct for selection bias that potentially arises when a population with only available exposure and outcome data is included as compared with a full initial cohort recruited at pregnancy, we used inverse probability weighting (Weisskopf et al. 2015; Weuve et al. 2012). In brief, we first imputed missing covariates for all eligible subjects ($n = 9{,}610$), and we then used all the available information to predict the probability of participation in the present study and used the inverse of those probabilities as weights in the analyses, which were then applied to the imputed data sets obtained in the previous step, so that results would be representative for the initial populations of the cohorts. The variables used to create the weights, as well as the distribution of the obtained weights, can be found in Figure S2.

After visual inspection of the distributions, we used linear regression models to analyze the relationships between concentrations of air pollutants first during pregnancy and then during childhood, with white matter microstructure metrics. We first performed single-pollutant analyses wherein each pollutant was studied separately. Next, we ran multipollutant analyses using the Deletion/Substitution/Addition (DSA) algorithm, which has shown relatively good performance with reference to a compromise between sensitivity and false discovery proportion compared with other similar methods (Agier et al. 2016). Briefly, the DSA algorithm is an iterative selection method that selects the variables that are most predictive of the outcome by cross-validation, taking into account the correlation matrix of the variables and simultaneously correcting for multiple testing. This algorithm allows three steps at each performed iteration, namely, *a*) deletion: removal of a variable; *b*) substitution: replacement of one variable with another one; and *c*) addition: insertion of a variable to the pending model. The exploration for the optimal model, with optimal model representing a combination of variables with the smallest value of root-mean-square deviation, begins with the intercept model and continues with the deletion, substitution, and addition process to identify the optimal combination of variables. To assure the adjustment for all potential confounding variables in each model, we fixed the potential confounders, allowing only the air pollution exposures to participate in the selection process. When two or more pollutants showed a correlation of 0.90 or more, we included only the pollutant that the LUR model showed had a better performance based on the R^2 of the model (see Table S2). Because the DSA algorithm is based on a cross-validation process that is subject to random variations, we ran each model 200 times, selecting the final model based on frequency of occurrence (at least 10%). We performed two separate analyses using the DSA algorithm: one including only air pollution exposures in pregnancy; and the second one including only the childhood air pollution exposures. In addition, for each global outcome, we performed a linear regression model that included all pregnancy and childhood exposures that were significant predictors of the outcome in a single-pollutant model and significant predictors of the outcome in a DSA-selected multipollutant model of pregnancy exposures or childhood exposures. In addition, the pollutants that were nominally significant in the multipollutant models of global FA or MD, as well as nominally significant in the single-pollutant models, were analyzed in separate single-pollutant models of FA and MD in 12 individual white matter tracts (Figure 1). Finally, if more than one pollutant remained significant for FA or MD in the same tract after application of false discovery rate (FDR) correction (Benjamini and Hochberg 1995), we performed multipollutant models for FA or MD in the tract.

Because we considered the address at birth as representative for the pregnancy period for those participants who were recruited shortly after birth and because their mothers were of slightly higher mean age {33.2 y [standard deviation (SD) = 4.8] vs. 30.9 y (SD = 4.8)}, and from a higher socioeconomic position as compared with mothers recruited during pregnancy (e.g., highest category education 57% vs. 53%; highest category household income: 76% vs. 64%), we repeated the pregnancy analyses excluding the children from mothers recruited shortly after birth, to test the sensitivity of the results. The pollutants analyzed were the same as those selected by the DSA algorithm in the analyses that included the full study population.

Finally, to quantify the measurement error in the air pollution assessment (LUR model predictions) and to transfer the resulting uncertainty to the exposure–outcome associations, we used a bootstrap method (Szpiro et al. 2011). Briefly, this method performs iteratively the following steps: *a*) simulates a new health outcome variable and the exposure at the monitoring locations based on the fitted models and residual errors; *b*) builds a new LUR model that predicts the simulated exposure; *c*) uses the new LUR model to predict exposure for the whole cohort; and *d*) estimates the exposure–outcome association with the newly generated health outcome variable and predicted exposure. The variance in the estimates resulting from the different iterations was used as the measurement error corrected variance. This variance or, equivalently, the confidence intervals (CIs) were compared with the variance obtained when measurement error was not taken into account. Given that the measurement error is expected to be mostly of Berkson type, bias in exposure–outcome coefficient estimates was not expected and was therefore not corrected (Szpiro et al. 2011).

All models were carried out with all imputed data sets (except for the DSA selection process and the measurement error calculations, which were carried out with the 25th imputed data set), were corrected for a potential selection bias using inverse probability weighting, and were adjusted for potential confounding variables described in the section above. We present beta coefficients and their 95% CIs per 20 $\mu g/m^3$ for NO_X; 10 $\mu g/m^3$ for NO_2; 10 $\mu g/m^3$ for PM_{10}; 5 $\mu g/m^3$ for PM_{coarse}; 5 $\mu g/m^3$ for $PM_{2.5}$; $10^{-5}/m$ for $PM_{2.5}$ absorbance; 1 ng/m^3 for PAHs; 0.1 ng/m^3 for B[a]P; 1 $\mu g/m^3$ for OC; 5 ng/m^3 for Cu in $PM_{2.5}$; 100 ng/m^3 for Fe in $PM_{2.5}$; 50 ng/m^3 for K in $PM_{2.5}$; 100 ng/m^3 for Si in $PM_{2.5}$; 10 ng/m^3 for Zn in $PM_{2.5}$; 1 nmol DTT/min/m^3 for OP_{DTT}; 1,000 arbitrary units/m^3 for OP_{ESR}; and 10,000 particles/cm^3 for UFP, based on the distribution of each exposure variable. Statistical tests of hypotheses were two-tailed with significance set at $p < 0.05$. Statistical analyses were carried out using STATA (version 14.0; StataCorporation) and R (version 3.4.2; R Development Core Team).

Table 1. Participant characteristics and comparison between included and non-included subjects in the study among the 9,610 eligible subjects.

	Distribution		
Participant characteristics	Included ($n = 2,954$)	Not included ($n = 6,656$)	p-Value
Maternal education level			<0.001
Primary education or lower	176 (6.5%)	775 (13.6%)	
Secondary education	1,092 (40.1%)	2,784 (48.8%)	
Higher education	1,453 (53.4%)	2,148 (37.6%)	
Missing	233	949	
Paternal education level			<0.001
Primary education or lower	92 (4.9%)	335 (10.2%)	
Secondary education	700 (37.6%)	1,420 (43.1%)	
Higher education	1,069 (57.4%)	1,542 (46.8%)	
Missing	1,093	3,359	
Monthly household income at intake			<0.001
<900€	172 (7.5%)	658 (15.2%)	
900€–1,600€	319 (13.8%)	891 (20.6%)	
1,600€–2,200€	329 (14.3%)	663 (15.3%)	
>2,200€	1,486 (64.4%)	2,110 (48.8%)	
Missing	648	2,334	
Maternal country of birth			<0.001
Netherlands	1,702 (58.7%)	2,766 (45.8%)	
Other Western	252 (8.7%)	516 (8.5%)	
Non-Western	944 (32.6%)	2,761 (45.7%)	
Missing	56	613	
Paternal country of birth			<0.001
Netherlands	1,419 (69.5%)	2,207 (57.2%)	
Other Western	120 (5.9%)	283 (7.3%)	
Non-Western	502 (24.6%)	1,368 (35.5%)	
Missing	913	2,798	
Family status at intake			<0.001
Married	1,394 (51.5%)	2,808 (49.1%)	
Living together	1,023 (37.8%)	1,989 (34.7%)	
No partner	292 (10.8%)	928 (16.2%)	
Missing	245	931	
Maternal parity (nulli- vs. multiparous)	1,630 (57.2%)	3,473 (54.3%)	<0.001
Missing	103	259	
Maternal smoking during pregnancy			<0.001
Never	2,004 (78.2%)	3,956 (71.3%)	
Smoking until pregnancy known	222 (8.7%)	470 (8.5%)	
Continued smoking during pregnancy	338 (13.2%)	1,123 (20.2%)	
Missing	390	1,107	
Maternal alcohol use during pregnancy			<0.001
Never	973 (41.7%)	2,773 (53.4%)	
Alcohol use until pregnancy known	335 (14.4%)	691 (13.3%)	
Continued alcohol use during pregnancy	1,023 (43.9%)	1,728 (33.3%)	
Missing	623	1,464	
Maternal age at intake (y)	31.2 (4.8)	29.3 (5.5)	<0.001
Missing	0	2	
Paternal age at intake (y)	33.5 (5.3)	32.3 (5.9)	<0.001
Missing	877	2,477	
Maternal prepregnancy BMI (kg/m^2)	23.4 (4.0)	23.8 (4.5)	0.003
Missing	773	1,815	
Paternal BMI (kg/m^2)	25.2 (3.3)	25.4 (3.6)	0.141
Missing	884	2,485	
Maternal height (cm)	168.1 (7.4)	166.7 (7.4)	<0.001
Missing	316	591	
Paternal height (cm)	182.6 (7.7)	181.1 (8.0)	<0.001
Missing	880	2,475	
Maternal psychological distress during pregnancy	0.3 (0.3)	0.3 (0.4)	<0.001
Missing	717	2,333	
Paternal psychological distress during pregnancy	0.1 (0.2)	0.2 (0.3)	<0.001
Missing	1,169	3,539	
Maternal IQ score	97.9 (14.7)	94.0 (15.7)	<0.001
Missing	266	3,077	
Child's sex (boy vs. girl)	1,472 (49.8%)	3,339 (50.2)	0.298
Missing	0	107	
Child's genetic ancestry[a]			
Principal component 1	7.4 (40.5)	−4.0 (48.1)	<0.001
Principal component 2	1.3 (20.9)	−0.7 (23.8)	0.002
Principal component 3	−2.6 (13.4)	1.4 (17.1)	<0.001
Principal component 4	−0.4 (10.4)	0.2 (12.6)	0.045
Missing	1,073	2,851	
Child's age at scanning session (y)	10.1 (0.6)	10.1 (0.6)	<0.001
Missing	0	5,722	

Note: Values are counts (percentages) for the categorical variables and mean (standard deviation) for the continuous variables. χ^2 test was used for categorical variables and Student's t-test for continuous variables. BMI, body mass index; IQ, intelligence quotient.
[a]Values are multiplied by 1,000.

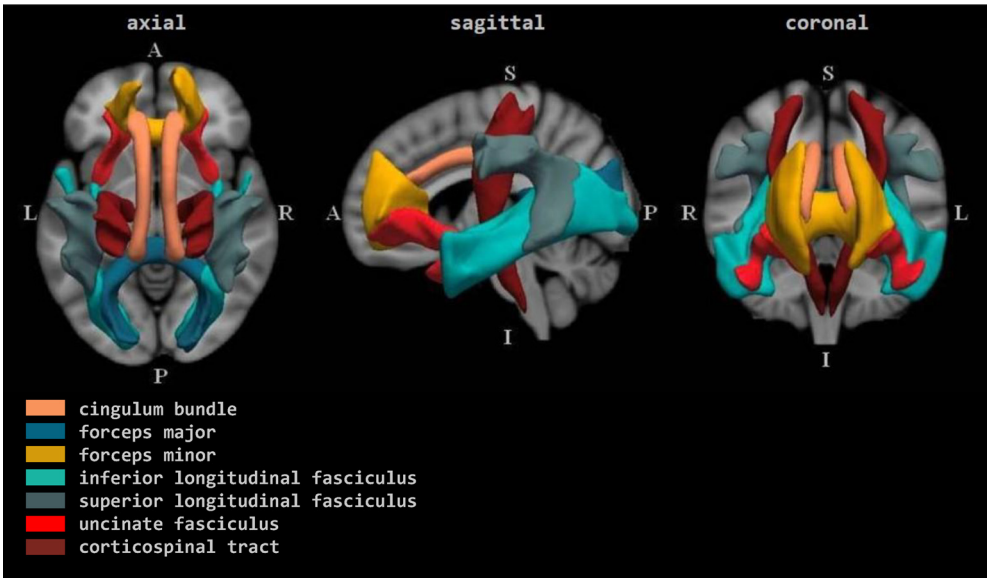

Figure 1. Group average representations of the tracts in standard coordinate space. Note: A, anterior; I, inferior; L, left; P, posterior; R, right; S, superior.

Results

Participant characteristics are shown in Table 1. The percentage of missing values was below 30% except for paternal country of birth, paternal education level, paternal psychological distress, and child genetics ancestry, which had 31%, 37%, 40%, and 36% of missing values respectively. Based on observations with known values, mothers of the included participants ($n = 2{,}954$) were more likely to have higher education, higher household income, be Dutch, and have a partner, as compared with mothers of participants that were not included ($n = 6{,}656$). Mean air pollution exposure concentrations during pregnancy were 35.1 $\mu g/m^3$ for NO_2 and 16.5 $\mu g/m^3$ for $PM_{2.5}$, and during childhood, 32.8 $\mu g/m^3$ for NO_2 and 16.4 $\mu g/m^3$ for $PM_{2.5}$ (Table 2). Correlations between the exposures in the two periods of interest were generally moderate, ranging between 0.40 for NO_2 and 0.63 for OC (Table 2). Mothers with a higher level of education and a higher monthly household income and who were nulliparous were exposed to higher average NO_2 concentrations during pregnancy. These associations were, however, not consistent between the different pollutants (see Tables S3–S11). Correlations between the concentrations of pollutants also varied considerably depending on the pollutant (see Figures S2 and S3). Based on the correlations, we excluded PM_{10}, B[a]P, K, and UFP from the multipollutant analysis because they showed correlations higher than 0.90 with $PM_{2.5}$ absorbance, PAHs, Zn, and Cu, respectively, but had a poorer performing LUR model [with exception of B[a]P, which had a better performing LUR model than PAHs (see Table S2) but was excluded because the PAH category comprises various polycyclic aromatic hydrocarbons, including B[a]P, and was therefore considered more comprehensive].

In the single-pollutant analysis, higher concentrations of NO_X, PM_{10}, $PM_{2.5}$, and $PM_{2.5}$ absorbance during pregnancy were significantly associated with lower global FA (Table 3). Higher concentrations of NO_X, NO_2, PM_{10}, $PM_{2.5}$, $PM_{2.5}$ absorbance, Cu, Fe, Si, OP_{ESR}, and UFP during pregnancy showed significant associations with higher global MD (Table 4). In the multipollutant analysis, $PM_{2.5}$ exposure during pregnancy remained significantly associated

Table 2. Air pollution exposure levels during pregnancy and during childhood, and Pearson's correlations between the exposures at the two time periods.

	Pregnancy				Childhood				
Pollutant	Mean	p25	p50	p75	Mean	p25	p50	p75	Correlation
NO_X	51.1	40.9	46.6	58.2	47.0	38.4	43.1	52.1	0.55
NO_2	34.7	31.9	34.2	36.7	32.6	29.4	32.5	35.1	0.47
PM_{10}	27.1	26.0	26.7	28.0	26.6	25.7	26.3	27.2	0.52
PM_{coarse}	9.9	9.2	10.1	10.6	9.5	8.6	9.5	10.3	0.56
$PM_{2.5}$	17.0	16.6	16.8	17.2	16.8	16.5	16.7	17.1	0.61
$PM_{2.5}$ abs	1.7	1.5	1.6	1.8	1.6	1.4	1.5	1.7	0.53
PAHs	1.0	0.8	0.9	1.1	1.0	0.8	0.9	1.1	0.66
B[a]P	0.1	0.1	0.1	0.1	0.1	0.1	0.1	0.1	0.67
OC	1.7	1.5	1.8	2.0	1.6	1.4	1.7	1.9	0.60
Cu	4.9	4.5	4.6	5.0	4.6	4.2	4.5	4.8	0.53
Fe	123.4	114.1	119.8	129.1	116.8	106.6	116.5	124.4	0.52
K	113.0	108.5	110.5	114.8	112.1	108.1	110.2	113.4	0.61
Si	93.0	87.9	88.8	90.5	91.6	87.6	88.6	90.4	0.60
Zn	20.2	17.6	18.8	21.3	20.0	17.4	18.7	20.8	0.55
OP_{DTT}	1.3	1.3	1.3	1.4	1.3	1.2	1.3	1.4	0.59
OP_{ESR}	1,079.4	1,000.7	1,036.6	1,100.1	1,037.9	964.7	1,014.7	1,072.2	0.57
UFP	10,330.3	9,509.9	10,058.5	10,926.3	9,547.1	8,446.0	9,644.8	10,385.0	0.49

Note: B[a]P, benzo[a]pyrene in ng/m^3; Cu, copper in ng/m^3; Fe, iron in ng/m^3; K, potassium in ng/m^3; NO_2, nitrogen dioxide in $\mu g/m^3$; NO_X, nitrogen oxides in $\mu g/m^3$; OC, organic carbon in ng/m^3; OP, oxidative potential (evaluated using two acellular methods: OP_{DTT}, dithiothreitol in nmol DTT/min/m^3, and OP_{ESR}, electron spin resonance in arbitrary units/m^3); PAHs, polycyclic aromatic hydrocarbons in ng/m^3; PM, particulate matter with different aerodynamic diameters: <10 μm (PM_{10}) in $\mu g/m^3$; between 10 μm and 2.5 μm (PM_{coarse}) in $\mu g/m^3$; <2.5 μm ($PM_{2.5}$) in $\mu g/m^3$; $PM_{2.5}$ abs, absorbance of $PM_{2.5}$ filters in $10^{-5}/m$; Si, silicon in ng/m^3; UFP, ultrafine particles in particles/cm^3; Zn, zinc in ng/m^3.

Table 3. Adjusted associations between exposure during pregnancy and childhood to single air pollutants and global fractional anisotropy at 9–12 years of age.

		Global fractional anisotropy					
		Pregnancy			Childhood		
Pollutant	Contrast	Coef.	95% CI	*p*-Value	Coef.	95% CI	*p*-Value
NO_X	20 $\mu g/m^3$	−0.11	−0.20, −0.02	0.018	−0.14	−0.23, −0.04	0.007
NO_2	10 $\mu g/m^3$	−0.11	−0.25, 0.03	0.1	−0.13	−0.25, −0.01	0.029
PM_{10}	10 $\mu g/m^3$	−0.49	−0.90, −0.08	0.018	−0.45	−0.91, 0.01	0.1
PM_{coarse}	5 $\mu g/m^3$	−0.05	−0.37, 0.27	0.8	−0.29	−0.63, 0.04	0.1
$PM_{2.5}$	5 $\mu g/m^3$	−0.71	−1.26, −0.16	0.012	−0.46	−1.14, 0.21	0.2
$PM_{2.5}$ abs	$10^{-5}/m$	−0.29	−0.51, −0.07	0.012	−0.27	−0.51, −0.02	0.032
PAHs	1 ng/m^3	0.01	−0.19, 0.21	1.0	0.15	−0.09, 0.38	0.2
B[a]P	0.1 ng/m^3	−0.06	−0.24, 0.13	0.6	0.11	−0.14, 0.35	0.4
OC	1 $\mu g/m^3$	−0.12	−0.29, 0.05	0.2	−0.20	−0.38, −0.03	0.024
Cu	5 ng/m^3	−0.32	−0.71, 0.06	0.1	−0.22	−0.65, 0.21	0.3
Fe	100 ng/m^3	−0.20	−0.54, 0.14	0.2	−0.22	−0.53, 0.09	0.2
K	50 ng/m^3	−0.38	−0.84, 0.08	0.1	−0.53	−1.03, −0.03	0.039
Si	100 ng/m^3	−0.28	−0.70, 0.15	0.2	−0.24	−0.66, 0.19	0.3
Zn	10 ng/m^3	−0.12	−0.28, 0.04	0.1	−0.13	−0.27, 0.02	0.1
OP_{DTT}	1 nmol DTT/min/m^3	0.21	−0.34, 0.75	0.4	−0.14	−0.69, 0.42	0.6
OP_{ESR}	1,000 units/m^3	−0.19	−0.55, 0.17	0.3	−0.21	−0.57, 0.16	0.3
UFP	10,000 particles/cm^3	−0.26	−0.63, 0.11	0.2	−0.21	−0.56, 0.15	0.3

Note: Coefficients and 95% CI from linear regression models adjusted for both maternal and paternal education, country of birth, age, height, BMI, and psychological distress during pregnancy; maternal smoking and alcohol consumption during pregnancy, parity, marital status, intelligence quotient, and household income; and child's genetic ancestry, gender, and age at the scanning session. Any missing covariates were imputed through multiple imputation, and inverse probability weighting technique was used to account for potential selection bias. B[a]P, benzo[a]pyrene; CI, confidence intervals; coef., coefficient; NO_2, nitrogen dioxide; NO_X, nitrogen oxides; OC, organic carbon; OP, oxidative potential (evaluated using two acellular methods: OP_{DTT}, dithiothreitol and OP_{ESR}, electron spin resonance); PAHs, polycyclic aromatic hydrocarbons; PM, particulate matter with different aerodynamic diameters: PM_{10}), <10 μm; PM_{coarse}, between 10 μm and 2.5 μm; $PM_{2.5}$, <2.5 μm; $PM_{2.5}$ abs, absorbance of $PM_{2.5}$ filters; UFP, ultrafine particles.

with global FA [0.71 lower global FA (95% CI: −1.26, −0.16) per 5-$\mu g/m^3$ increase of $PM_{2.5}$] (Table 5). $PM_{2.5}$ and PAH exposures during pregnancy were both significant predictors of global FA when included in the same model, showing inverse and positive associations, respectively. Exposure in pregnancy to Si remained significantly associated with global MD in the multipollutant analysis [0.06 higher global MD (95% CI: 0.01, 0.11) per 100-ng/m^3 increase of Si]. Exclusion of children with mothers recruited shortly after the pregnancy ($n = 310$) did not lead to notable changes in the effect estimates (see Table S12).

Regarding air pollution exposure during childhood, higher concentrations of NO_X, NO_2, $PM_{2.5}$ absorbance, OC, and K were significantly associated with lower global FA (Table 3). Higher concentrations of NO_X, NO_2, PM_{10}, PM_{coarse}, $PM_{2.5}$, $PM_{2.5}$ absorbance, K, Si, Zn, and OP_{DTT} showed significant associations with higher global MD (Table 4). In the multipollutant analysis, childhood exposure to NO_X remained significantly associated with global FA [0.14 lower global FA (95% CI: −0.23, −0.04) per 20-$\mu g/m^3$ increase of NO_X], whereas Zn and OP_{DTT} remained significantly associated with global MD [0.03 higher global MD (95% CI: 0.01, 0.04) per 10-ng/m^3 increase in Zn, and 0.07 higher MD (95% CI: 0.00, 0.44) per 1-nmol DTT/min/m^3 increase in OP_{DTT}] (Table 5).

When pregnancy $PM_{2.5}$ and childhood NO_X exposures that were nominally significant in the multipollutant models, and nominally significant in the single-pollutant models, were analyzed simultaneously, they no longer showed statistically significant associations with global FA (see Table S13), and the beta coefficients approached zero. However, the associations between pregnancy

Table 4. Adjusted associations between exposure during pregnancy and childhood to single air pollutants and global mean diffusivity at 9–12 years of age.

		Global mean diffusivity					
		Pregnancy			Childhood		
Pollutant	Contrast	Coef.	95% CI	*p*-Value	Coef.	95% CI	*p*-Value
NO_X	20 $\mu g/m^3$	0.01	0.00, 0.02	0.1	0.02	0.01, 0.03	0.005
NO_2	10 $\mu g/m^3$	0.02	0.00, 0.04	0.021	0.02	0.00, 0.03	0.011
PM_{10}	10 $\mu g/m^3$	0.05	0.00, 0.10	0.042	0.07	0.01, 0.12	0.027
PM_{coarse}	5 $\mu g/m^3$	0.03	−0.01, 0.07	0.2	0.04	0.00, 0.09	0.038
$PM_{2.5}$	5 $\mu g/m^3$	0.09	0.02, 0.15	0.014	0.11	0.03, 0.20	0.010
$PM_{2.5}$ abs	$10^{-5}/m$	0.04	0.01, 0.06	0.012	0.04	0.01, 0.07	0.009
PAHs	1 ng/m^3	0.01	−0.01, 0.04	0.3	0.01	−0.02, 0.04	0.5
B[a]P	0.1 ng/m^3	0.02	−0.01, 0.04	0.1	0.01	−0.02, 0.04	0.3
OC	1 $\mu g/m^3$	0.02	−0.01, 0.04	0.2	0.02	0.00, 0.04	0.1
Cu	5 ng/m^3	0.05	0.01, 0.10	0.030	0.03	−0.02, 0.09	0.2
Fe	100 ng/m^3	0.05	0.01, 0.09	0.018	0.03	−0.01, 0.07	0.1
K	50 ng/m^3	0.04	−0.02, 0.09	0.2	0.09	0.03, 0.15	0.006
Si	100 ng/m^3	0.07	0.02, 0.12	0.010	0.05	0.00, 0.11	0.047
Zn	10 ng/m^3	0.01	−0.01, 0.03	0.2	0.03	0.01, 0.05	0.003
OP_{DTT}	1 nmol DTT/min/m^3	0.06	−0.01, 0.13	0.069	0.09	0.02, 0.16	0.016
OP_{ESR}	1,000 units/m^3	0.04	0.00, 0.09	0.047	0.04	0.00, 0.09	0.1
UFP	10,000 particles/cm^3	0.05	0.01, 0.10	0.023	0.03	−0.01, 0.08	0.1

Note: Coefficients and 95% CI from linear regression models adjusted for both maternal and paternal education, country of birth, age, height, BMI, and psychological distress during pregnancy; maternal smoking and alcohol consumption during pregnancy, parity, marital status, intelligence quotient, and household income; and child's genetic ancestry, gender, and age at the scanning session. Any missing covariates were imputed through multiple imputation, and inverse probability weighting technique was used to account for potential selection bias. B[a]P, benzo[a]pyrene; BMI, body mass index; CI, confidence intervals; coef., coefficient; NO_2, nitrogen dioxide; NO_X, nitrogen oxides; OC, organic carbon; OP, oxidative potential (evaluated using two acellular methods: OP_{DTT}, dithiothreitol and OP_{ESR}, electron spin resonance); PAHs, polycyclic aromatic hydrocarbons; PM, particulate matter with different aerodynamic diameters: PM_{10}, <10 μm; PM_{coarse}, between 10 μm and 2.5 μm; $PM_{2.5}$, $PM_{2.5}$, <2.5 μm; $PM_{2.5}$ abs, absorbance of $PM_{2.5}$ filters; UFP, ultrafine particles.

Table 5. Results of multipollutant models selected by the Deletion/Substitution/Addition algorithm for pregnancy and childhood exposures in relation to global fractional anisotropy and global mean diffusivity, respectively.

Exposure models	Contrast	Coef. (95% CI)	*p*-Value
Global fractional anisotropy			
Pregnancy exposure models (% of runs)			
Model 1 (24.5%)			
$PM_{2.5}$	5 $\mu g/m^3$	−1.49 (−2.25, −0.73)	<0.001
PAHs	1 ng/m^3	0.33 (0.06, 0.59)	0.017
OP_{DTT}	1 nmol DTT/min/m^3	0.50 (−0.07, 1.07)	0.1
Model 2 (20%)			
$PM_{2.5}$	5 $\mu g/m^3$	−1.32 (−2.06, −0.58)	<0.001
PAHs	1 ng/m^3	0.33 (0.06, 0.60)	0.017
Model 3 (13%)			
$PM_{2.5}$	5 $\mu g/m^3$	−0.71 (−1.26, −0.16)	0.012
Childhood exposure models (% of runs)			
Model 1 (22.5%)			
NO_X	20 $\mu g/m^3$	−0.14 (−0.23, −0.04)	0.007
Model 2 (10.5%)			
NO_X	20 $\mu g/m^3$	−0.13 (−0.24, −0.03)	0.015
OP_{DTT}	1 nmol DTT/min/m^3	0.46 (−0.19, 1.11)	0.2
OC	1 $\mu g/m^3$	−0.19 (−0.40, 0.01)	0.1
Global mean diffusivity			
Pregnancy exposure models (% of runs)			
Model 1 (13.5%)			
Si	100 ng/m^3	0.06 (0.01, 0.11)	0.018
OP_{DTT}	1 nmol DTT/min/m^3	0.05 (−0.02, 0.11)	0.2
Childhood exposure models (% of runs)			
Model 1 (46.5%)			
Zn	10 ng/m^3	0.03 (0.01, 0.04)	0.005
OP_{DTT}	1 nmol DTT/min/m^3	0.07 (0.00, 0.14)	0.046
Model 2 (23%)			
Zn	10 ng/m^3	0.02 (0.01, 0.04)	0.008
OP_{DTT}	1 nmol DTT/min/m^3	0.06 (−0.01, 0.13)	0.1
Si	100 ng/m^3	0.04 (−0.02, 0.09)	0.2

Note: Model selection was performed using Deletion/Substitution/Addition algorithm. PM_{10}, B[a]P, K, and UFPs were excluded due to a correlation of 0.90 or more with $PM_{2.5}$ absorbance, PAHs, Zn, and Cu respectively. For each combination of period of exposure and outcome, 200 runs were performed and the final model was selected based on frequency of occurrence (percentage of runs, at least 10% to be reported here). Coefficients and 95% CI from (multiple) linear regression models adjusted for both maternal and paternal education, country of birth, age, height, BMI, and psychological distress during pregnancy; maternal smoking and alcohol consumption during pregnancy, parity, marital status, intelligence quotient, and household income; and child's genetic ancestry, gender, and age at the scanning session. Any missing covariates were imputed through multiple imputation, and inverse probability weighting technique was used to account for potential selection bias. B[a]P, benzo[a]pyrene; BMI, body mass index; CI, confidence intervals; coef., coefficient; Cu, copper; K, potassium; NO_X, nitrogen oxides; OC, organic carbon; OP_{DTT}, oxidative potential of $PM_{2.5}$ (DTT: evaluated using dithiothreitol); PAHs, polycyclic aromatic hydrocarbons; $PM_{2.5}$, particulate matter with diameter of <2.5 μm; Si, silicon; UFPs, ultrafine particles; Zn, zinc.

exposure to Si and childhood exposure to Zn and global MD remained significant after mutual adjustment, and the beta coefficients did not change notably.

Analyses of FA in the 12 specific white matter tracts did not indicate FDR-significant associations with pregnancy $PM_{2.5}$ or childhood NO_X in any tract (see Table S14). In analyses of MD in specific white matter tracts, FDR-significant associations were estimated for pregnancy Si and MD in the cingulate gyrus part of the cingulum of the left hemisphere, the superior longitudinal fasciculus of the left hemisphere, and the forceps minor. Associations between childhood Zn and MD were FDR-significant for 6 tracts: the uncinate fasciculus tract of the right hemisphere, the cingulate gyrus part of the cingulum of both hemispheres, the superior longitudinal fasciculus of both hemispheres, and the forceps minor (see Table S15). None of the coefficients for childhood OP_{DTT} and MD in specific tracts were FDR-significant. When we simultaneously modeled pregnancy Si and childhood Zn in association with MD in the 3 tracts that were FDR-significant for both pollutants in single-pollutant models, associations were nominally significant for both exposures in all 3 tracts (see Table S16). Accounting for measurement error only slightly increased the standard errors and did not alter the main conclusions (see Table S17).

Discussion

We observed associations between exposure to air pollutants in two critical periods of brain development, namely pregnancy and childhood, and white matter microstructure in preadolescents 9–12 years of age. Our multipollutant analysis identified statistically significant associations between exposure to $PM_{2.5}$ and elemental Si during pregnancy and exposure to NO_X, elemental Zn, and OP_{DTT} during childhood and white matter microstructure, associations that were also statistically significant in the single-pollutant model analyses. When pregnancy $PM_{2.5}$ and childhood NO_X were included in the same model, the associations with global FA were no longer statistically significant. However, when pregnancy Si and childhood Zn and OP_{DTT} were included in the same model, associations of pregnancy Si and childhood Zn with global MD remained statistically significant. Higher exposures to pollutants were predominantly related to lower FA and higher MD, generally considered as indicators for atypical white matter microstructure and previously associated with psychiatric and neurological disorders (White et al. 2008, Aoki et al. 2017; van Ewijk et al. 2012).

Among pregnancy exposures that were significantly associated with white matter microstructure in single-pollutant models and were selected for multipollutant models by the DSA algorithm, $PM_{2.5}$ remained significantly associated with lower global FA. Exposure to $PM_{2.5}$ is a human health concern, with associated health effects including those in neurological and neuropsychological domains, among many others (Beelen et al. 2014; Block et al. 2012; Chen et al. 2017; Kaufman et al. 2016; Pedersen et al. 2013; Raaschou-Nielsen et al. 2013). Although single-pollutant models of global FA were not significant for pregnancy PAHs, the DSA algorithm selected models that estimated significant associations

for both pregnancy $PM_{2.5}$ and pregnancy PAHs, with PAHs showing a significant positive association with global FA in the multipollutant model, whereas it showed no significant association in the single-pollutant model. One possible explanation for these unexpected results with PAHs could be that the mutually adjusted estimates may have been affected by collinearity. However, the two exposures were only moderately correlated ($r = 0.66$).

Pregnancy exposure to Si was a significant predictor of global MD in a multipollutant model that also included childhood Zn and OP_{DTT}. Pregnancy exposure to Si was also an FDR-significant predictor for MD in three white matter tracts based on single-pollutant models, and the associations remained statistically significant when we adjusted the models for childhood exposure to Zn. Si has not been documented as a potential neurotoxicant to date. However, Si may be a marker of exposure to resuspended road dust (Viana et al. 2008), and associations with Si may therefore reflect associations with exposure to high traffic rather than exposure to Si specifically.

In analyses of exposures to air pollution during childhood, the association between higher concentrations of NO_X and lower global FA remained significant in the multipollutant analysis. In Europe, the predominant source of NO_X gasses in the air is an incomplete combustion of hydrocarbons originating mainly from diesel fuel (Cyrys et al. 2003). Exposure to diesel exhaust has been linked to numerous adverse health effects, such as increased risk of neuroinflamation (Block et al. 2012). Results of the multipollutant analysis also suggested a robust association between higher childhood exposure to Zn, a marker for brake linings and tire wear (Viana et al. 2008), and higher global MD. The association between higher childhood exposure to Zn and higher global MD was further supported by identification of six white matter tracts, including association and callosal tracts and tracts of the limbic system. These results are location-wise moderately in accordance with findings of our previous study wherein we found an association between higher concentrations of air pollution during pregnancy and thinner cerebral cortex in precuneus and rostral middle frontal regions in children 6–10 years of age (Guxens et al. 2018). Zn is a vital trace element for proper brain development processes and brain functions later in life (Gower-Winter and Levenson 2012); however, its accumulation in the brain can cause excitotoxicity, oxidative stress, and impairment of the generation of cellular energy (Gower-Winter and Levenson 2012). We also observed an association in single-pollutant, as well as multipollutant models, between childhood exposure to a higher oxidative potential of $PM_{2.5}$, which is a measure to quantify the potentiality of $PM_{2.5}$ to induce oxidative stress, and higher global MD. Oxidative stress together with inflammation and chronic activation of the hypothalamic–pituitary–adrenal axis account for the most likely mechanisms through which air pollutants can cause damage to the brain (Block et al. 2012; Thomson 2013).

To our knowledge, there has been only one previous epidemiological study of associations between air pollution and white matter microstructure (Pujol et al. 2016b). In that study, that exposure to higher concentrations of Cu at schools was associated with higher FA in regions adjacent to the caudate nucleus in children 8–12 years of age. Similar to Zn, Cu reflects brake linings (Viana et al. 2008). In our study, we did not find a significant association between pregnancy or childhood exposure to Cu and FA, and the obtained nonsignificant associations were inverse, relating higher exposure to Cu to lower FA. The discrepancies in the results between the study of Pujol et al. (2016b) and our study might be attributable to differences in exposure assessment with respect to location and timing (school levels at 8–10 years of age vs. residential levels during pregnancy and from birth until 9–12 years of age), different Cu concentrations (8.7 ng/m^3 vs. 4.7 ng/m^3), or differences in sample size (263 vs. 2,954 children).

Our study has a number of considerable strengths: *a*) a large sample size for a population-based neuroimaging study in an urban setting; *b*) the use of advanced statistical methods, including inverse probability weighting to reduce possible selection and attrition bias in the study; *c*) the adjustment for various socioeconomic and lifestyle variables that are known to be potentially associated with air pollution exposure and brain structure in children; *d*) a standardized and validated air pollution assessment in two key developmental periods with insufficiently large measurement error to bias the health effect estimates; and *e*) a large number of simultaneously assessed pollutants in an advanced multipollutant approach. Correlations between the exposures during pregnancy and during childhood were only moderate, allowing us to disentangle associations in these two periods.

There are also several limitations in our study. Sampling campaigns were carried out when children were between 3.5 and 9 years of age and historical pollution data the study areas was not available for all the pollutants to extrapolate the concentrations to the specific periods of interest. We therefore assumed that the concentrations of the pollutants remained spatially stable over time based on previous research supporting stability of spatial contrast in air pollution demonstrated in the Netherlands for a period up to 8 y (1999–2007) (Eeftens et al. 2011) and in Great Britain for a period up to 18 y (1991–2009) (Gulliver et al. 2013). Another limitation of this study is the high correlation between some of the pollutants. We used an advanced variable selection technique that has demonstrated better performance with reference to a compromise between sensitivity and false discovery proportion compared with alternative methods in settings comparable to ours (Agier et al. 2016). Nevertheless, we still obtained an implausible result with pregnancy PAHs being selected by the DSA algorithm and showing a significant positive association with global FA when analyzed simultaneously with pregnancy $PM_{2.5}$ in a multipollutant model, whereas it showed no significant association in the single-pollutant analysis. Further methodological research is still needed to unequivocally identify specific pollutants of a complex mixture, particularly if they are derived from the same source. In addition, despite the careful and comprehensive selection of potential confounding variables, we cannot discard the possibility of residual confounding of other variables that we either did not consider or we considered but were unable to include due to poor measurement or lack of measurement, such as a perfect control for socioeconomic status. Residual confounding could introduce bias and thereby lead to incorrect estimates of the main associations (Weisskopf et al. 2018). In addition, several potential confounding variables, as well as variables used to predict participation in the study, had a high percentage of missing values. We applied multiple imputation, followed by inverse probability weighting to reduce possible selection and attrition bias in the study, but it is possible that this might not have been sufficient to entirely eliminate the bias due to missing covariates as well as missing variables used to calculate the inverse probability weights. Finally, lower FA and higher MD have generally been associated with impaired neurodevelopment and have been related to psychiatric and neurological disorders such as autism spectrum disorder and attention deficit hyperactivity disorder (Aoki et al. 2017; van Ewijk et al. 2012). However, the brain is a highly complicated organ, which undergoes many developmental processes, many of which take place simultaneously, and healthy progression of such processes can sometimes have opposing characteristics (Di Martino et al. 2014). Therefore, our results should be interpreted with caution.

In summary, we found an association between higher exposure to air pollutants representative of brake linings, tire wear, and tailpipe emissions originating mainly from diesel combustion with lower FA and higher MD of white matter in preadolescents. The observed associations involved exposure to air pollution

during both key developmental periods, namely, pregnancy and childhood, demonstrating the importance of examination of both periods in future studies. All pollutants showing associations have traffic as their main source and are, therefore, highly ubiquitous in urban settings, putting a very large portion of children at risk. Based on our results, the current direction toward innovative solutions for cleaner energy vehicles are strongly supported by the authors. However, these measures might not be completely adequate to mitigate health problems attributable to traffic-related air pollution given that we also observed associations with elemental zinc, which is a marker for brake linings and tire wear. Further studies are warranted to confirm these results.

Acknowledgments

The authors thank J. Barrera from ISGlobal for his generous help with improvements of the syntax for the multipollutant models performed in R. We also gratefully acknowledge the contribution of the children and parents, general practitioners, hospitals, midwives and pharmacies in Rotterdam for their participation in the Generation R Study.

Research described in this article was conducted under contract to the Health Effects Institute (HEI), an organization jointly funded by the U.S. Environmental Protection Agency (EPA) and certain motor vehicle and engine manufacturers. The content of this article does not necessarily reflect the views of HEI, or its sponsors, nor does it necessarily reflect the views and policies of the U.S. EPA or motor vehicle and engine manufacturers.

The Generation R Study is conducted by the Erasmus Medical Center in close collaboration with the School of Law and Faculty of Social Sciences of the Erasmus University Rotterdam, Rotterdam; the Municipal Health Service Rotterdam Area, Rotterdam; the Rotterdam Homecare Foundation, Rotterdam; and the Stichting Trombosedienst and Artsenlaboratorium Rijnmond (STAR-MDC), Rotterdam. The general design of the Generation R Study is made possible by financial support from the Erasmus Medical Center, Rotterdam; the Erasmus University Rotterdam; Netherlands Organization for Health Research and Development (ZonMw); the Netherlands Organization for Scientific Research (NWO); and the Ministry of Health, Welfare and Sport. Air pollution exposure assessment was made possible by funding from the European Community's Seventh Framework Program (Grant Agreement no. 211250, Grant Agreement no. 243406). In addition, the study was made possible by financial support from the ZonMw (Geestkracht Program 10.000.1003 and TOP 40-00812-98-11021). Neuroimaging was supported by the ZonMw TOP project no. 91211021 to T.W., Sophia Foundation Project S18-20 to R.L.M., and super computing computations for imaging processing were supported by the NWO Physical Sciences Division (Exacte Wetenschappen) and SURFsara (Cartesius compute cluster, https://www.surf.nl). Research described in this article was also conducted under contract to the HEI, an organization jointly funded by the U.S. EPA (Assistance Award No. R-82811201) and certain motor vehicle and engine manufacturers. The contents of this article do not necessarily reflect the views of HEI, or its sponsors, nor do they necessarily reflect the views and policies of the U.S. EPA or motor vehicle and engine manufacturers. V.W.V.J. and H.T. received funding from the ZonMw (VIDI 016.136.361 and NWO-grant 016.VICI.170.200, respectively), the European Research Council (ERC-2014-CoG-64916), and the European Union's Horizon 2020 research and innovation program under grant agreement no. 633595 (DynaHEALTH) and no. 733206 (LifeCycle). H.E.M. was supported by Stichting Volksbond Rotterdam and the Dutch Brain Foundation (De Hersenstichting, project number GH2016.2.01), and by the 2019 NARSAD Young Investigator Grant from the Brain and Behavior Research Foundation. M.G. is funded by a Miguel Servet fellowship (MS13/00054, CP13/00054, CI18/00018) awarded by the Spanish Institute of Health Carlos III. W.D. is funded in part by the Research Council of Norway (RCN) (grant 249779) and through the RCN Centers of Excellence funding scheme (grant 262700).

The funding organizations for this study had no involvement in the design and conduct of the study; collection, management, analysis, and interpretation of the data; preparation, review, or approval of the manuscript; or the decision to submit the manuscript for publication.

References

Agier L, Portengen L, Chadeau-Hyam M, Basagaña X, Giorgis-Allemand L, Siroux V, et al. 2016. A systematic comparison of linear regression–based statistical methods to assess exposome-health associations. Environ Health Perspect 124(12):1848–1856, PMID: 27219331, https://doi.org/10.1289/EHP172.

Aoki Y, Yoncheva YN, Chen B, Nath T, Sharp D, Lazar M, et al. 2017. Association of white matter structure with autism spectrum disorder and attention-deficit/hyperactivity disorder. JAMA Psychiatry 74(11):1120–1128, PMID: 28877317, https://doi.org/10.1001/jamapsychiatry.2017.2573.

Beelen R, Raaschou-Nielsen O, Stafoggia M, Andersen ZJ, Weinmayr G, Hoffmann B, et al. 2014. Effects of long-term exposure to air pollution on natural-cause mortality: an analysis of 22 European cohorts within the multicentre ESCAPE project. Lancet 383(9919):785–795, PMID: 24332274, https://doi.org/10.1016/S0140-6736(13)62158-3.

Behrens TEJ, Johansen-Berg H, Jbabdi S, Rushworth MFS, Woolrich MW. 2007. Probabilistic diffusion tractography with multiple fibre orientations: what can we gain? Neuroimage 34(1):144–155, PMID: 17070705, https://doi.org/10.1016/j.neuroimage.2006.09.018.

Behrens TEJ, Woolrich MW, Jenkinson M, Johansen-Berg H, Nunes RG, Clare S, et al. 2003. Characterization and propagation of uncertainty in diffusion-weighted MR imaging. Magn Reson Med 50(5):1077–1088, PMID: 14587019, https://doi.org/10.1002/mrm.10609.

Benjamini Y, Hochberg Y. 1995. Controlling the false discovery rate: a practical and powerful approach to multiple testing. J R Stat Soc Series B Methodol 57(1):289–300, https://doi.org/10.1111/j.2517-6161.1995.tb02031.x.

Block ML, Elder A, Auten RL, Bilbo SD, Chen H, Chen J-C, et al. 2012. The outdoor air pollution and brain health workshop. Neurotoxicology 33(5):972–984, PMID: 22981845, https://doi.org/10.1016/j.neuro.2012.08.014.

Calderón-Garcidueñas L, Engle R, Mora-Tiscareño A, Styner M, Gómez-Garza G, Zhu H, et al. 2011. Exposure to severe urban air pollution influences cognitive outcomes, brain volume and systemic inflammation in clinically healthy children. Brain Cogn 77(3):345–355, PMID: 22032805, https://doi.org/10.1016/j.bandc.2011.09.006.

Calderón-Garcidueñas L, Mora-Tiscareño A, Ontiveros E, Gómez-Garza G, Barragán-Mejía G, Broadway J, et al. 2008. Air pollution, cognitive deficits and brain abnormalities: a pilot study with children and dogs. Brain Cogn 68(2):117–127, PMID: 18550243, https://doi.org/10.1016/j.bandc.2008.04.008.

Chen H, Kwong JC, Copes R, Tu K, Villeneuve PJ, van Donkelaar A, et al. 2017. Living near major roads and the incidence of dementia, Parkinson's disease, and multiple sclerosis: a population-based cohort study. Lancet 389(10070):718–726, PMID: 28063597, https://doi.org/10.1016/S0140-6736(16)32399-6.

Cook PA, Bai Y, Nedjati-Gilani S, Seunarine KK, Hall MG, Parker GJ, et al. 2006. Camino: open-source diffusion-MRI reconstruction and processing. In: *Proceeding of the 14th Scientific Meeting of the International Society for Magnetic Resonance in Medicine*. Seattle, WA: ISMRM, 2759.

Cyrys J, Heinrich J, Hoek G, Meliefste K, Lewné M, Gehring U, et al. 2003. Comparison between different traffic-related particle indicators: elemental carbon (EC), $PM_{2.5}$ mass and absorbance. J Expos Sci Environ Epidemiol 13(2):134–143, PMID: 12679793, https://doi.org/10.1038/sj.jea.7500262.

De Beurs E. 2004. *Brief Symptom Inventory, Handleiding* [in Dutch]. Leiden, the Netherlands: PITS B.V.

de Groot M, Ikram MA, Akoudad S, Krestin GP, Hofman A, van der Lugt A, et al. 2015. Tract-specific white matter degeneration in aging: the Rotterdam Study. Alzheimers Dement 11(3):321–330, PMID: 25217294, https://doi.org/10.1016/j.jalz.2014.06.011.

de Hoogh K, Wang M, Adam M, Badaloni C, Beelen R, Birk M, et al. 2013. Development of land use regression models for particle composition in twenty study areas in Europe. Environ Sci Technol 47(11):5778–5786, PMID: 23651082, https://doi.org/10.1021/es400156t.

Di Martino A, Fair DA, Kelly C, Satterthwaite TD, Castellanos FX, Thomason ME, et al. 2014. Unraveling the miswired connectome: a developmental perspective. Neuron 83(6):1335–1353, PMID: 25233316, https://doi.org/10.1016/j.neuron.2014.08.050.

Dimond D, Schuetze M, Smith RE, Dhollander T, Cho I, Vinette S, et al. 2019. Reduced white matter fiber density in autism spectrum disorder. Cereb Cortex 29(4):1778–1788, PMID: 30668849, https://doi.org/10.1093/cercor/bhy348.

Eeftens M, Beelen R, Fischer P, Brunekreef B, Meliefste K, Hoek G. 2011. Stability of measured and modelled spatial contrasts in NO_2 over time. Occup Environ Med 68(10):765–770, PMID: 21285243, https://doi.org/10.1136/oem.2010.061135.

Gower-Winter SD, Levenson CW. 2012. Zinc in the central nervous system: from molecules to behavior. Biofactors 38(3):186–193, PMID: 22473811, https://doi.org/10.1002/biof.1012.

Grandjean P, Landrigan P. 2014. Neurobehavioural effects of developmental toxicity. Lancet Neurol 13(3):330–338, PMID: 24556010, https://doi.org/10.1016/S1474-4422(13)70278-3.

Gulliver J, de Hoogh K, Hansell A, Vienneau D. 2013. Development and back-extrapolation of NO_2 land use regression models for historic exposure assessment in Great Britain. Environ Sci Technol 47(14):7804–7811, PMID: 23763440, https://doi.org/10.1021/es4008849.

Guxens M, Lubczyńska MJ, Muetzel RL, Dalmau-Bueno A, Jaddoe VWV, Hoek G, et al. 2018. Air pollution exposure during fetal life, brain morphology, and cognitive function in school-age children. Biol Psychiatry 84(4):295–303, PMID: 29530279, https://doi.org/10.1016/j.biopsych.2018.01.016.

Jedynska A, Hoek G, Wang M, Eeftens M, Cyrys J, Keuken M, et al. 2014. Development of land use regression models for elemental, organic carbon, PAH, and hopanes/steranes in 10 ESCAPE/TRANSPHORM European study areas. Environ Sci Technol 48(24):14435–14444, PMID: 25317817, https://doi.org/10.1021/es502568z.

Jenkinson M, Beckmann CF, Behrens TEJ, Woolrich MW, Smith SM. 2012. FSL. Neuroimage 62(2):782–790, PMID: 21979382, https://doi.org/10.1016/j.neuroimage.2011.09.015.

Kaufman JD, Adar SD, Barr RG, Budoff M, Burke GL, Curl CL, et al. 2016. Association between air pollution and coronary artery calcification within six metropolitan areas in the USA (the Multi-Ethnic Study of Atherosclerosis and Air Pollution): a longitudinal cohort study. Lancet 388(10045):696–704, PMID: 27233746, https://doi.org/10.1016/S0140-6736(16)00378-0.

Kooijman MN, Kruithof CJ, van Duijn CM, Duijts L, Franco OH, van IJzendoorn MH, et al. 2016. The Generation R Study: design and cohort update 2017. Eur J Epidemiol 31(12):1243–1264, PMID: 28070760, https://doi.org/10.1007/s10654-016-0224-9.

Montagne DR, Hoek G, Klompmaker JO, Wang M, Meliefste K, Brunekreef B. 2015. Land use regression models for ultrafine particles and black carbon based on short-term monitoring predict past spatial variation. Environ Sci Technol 49(14):8712–8720, PMID: 26079151, https://doi.org/10.1021/es505791g.

Mortamais M, Pujol J, van Drooge BL, Macià D, Martínez-Vilavella G, Reynes C, et al. 2017. Effect of exposure to polycyclic aromatic hydrocarbons on basal ganglia and attention-deficit hyperactivity disorder symptoms in primary school children. Environ Int 105:12–19, PMID: 28482185, https://doi.org/10.1016/j.envint.2017.04.011.

Muetzel RL, Blanken LME, van der Ende J, El Marroun H, Shaw P, Sudre G, et al. 2018. Tracking brain development and dimensional psychiatric symptoms in children: a longitudinal population-based neuroimaging study. Am J Psychiatry 175(1):54–62, PMID: 28817944, https://doi.org/10.1176/appi.ajp.2017.16070813.

Neumann A, Noppe G, Liu F, Kayser M, Verhulst FC, Jaddoe VWV, et al. 2017. Predicting hair cortisol levels with hair pigmentation genes: a possible hair pigmentation bias. Sci Rep 7(1):8529, PMID: 28819144, https://doi.org/10.1038/s41598-017-07034-w.

Pedersen M, Giorgis-Allemand L, Bernard C, Aguilera I, Andersen A-MN, Ballester F, et al. 2013. Ambient air pollution and low birthweight: a European cohort study (ESCAPE). Lancet Respir Med 1(9):695–704, PMID: 24429273, https://doi.org/10.1016/S2213-2600(13)70192-9.

Peterson BS, Rauh VA, Bansal R, Hao X, Toth Z, Nati G, et al. 2015. Effects of prenatal exposure to air pollutants (polycyclic aromatic hydrocarbons) on the development of brain white matter, cognition, and behavior in later childhood. JAMA Psychiatry 72(6):531–540, PMID: 25807066, https://doi.org/10.1001/jamapsychiatry.2015.57.

Price AL, Patterson NJ, Plenge RM, Weinblatt ME, Shadick NA, Reich D. 2006. Principal components analysis corrects for stratification in genome-wide association studies. Nat Genet 38(8):904–909, PMID: 16862161, https://doi.org/10.1038/ng1847.

Pujol J, Fenoll R, Macià D, Martínez-Vilavella G, Alvarez-Pedrerol M, Rivas I, et al. 2016a. Airborne copper exposure in school environments associated with poorer motor performance and altered basal ganglia. Brain Behav 6(6):e00467, PMID: 27134768, https://doi.org/10.1002/brb3.467.

Pujol J, Martínez-Vilavella G, Macià D, Fenoll R, Alvarez-Pedrerol M, Rivas I, et al. 2016b. Traffic pollution exposure is associated with altered brain connectivity in school children. Neuroimage 129:175–184, PMID: 26825441, https://doi.org/10.1016/j.neuroimage.2016.01.036.

Raaschou-Nielsen O, Andersen ZJ, Beelen R, Samoli E, Stafoggia M, Weinmayr G, et al. 2013. Air pollution and lung cancer incidence in 17 European cohorts: prospective analyses from the European Study of Cohorts for Air Pollution Effects (ESCAPE). Lancet Oncol 14(9):813–822, PMID: 23849838, https://doi.org/10.1016/S1470-2045(13)70279-1.

Raven JC. 1962. *Advanced progressive matrices: Sets I and II.* London, UK: H.K. Lewis.

Schmithorst VJ, Yuan W. 2010. White matter development during adolescence as shown by diffusion MRI. Brain Cogn 72(1):16–25, PMID: 19628324, https://doi.org/10.1016/j.bandc.2009.06.005.

Suades-González E, Gascon M, Guxens M, Sunyer J. 2015. Air pollution and neuropsychological development: a review of the latest evidence. Endocrinology 156(10):3473–3482, PMID: 26241071, https://doi.org/10.1210/en.2015-1403.

Szpiro AA, Sheppard L, Lumley T. 2011. Efficient measurement error correction with spatially misaligned data. Biostatistics 12(4):610–623, PMID: 21252080, https://doi.org/10.1093/biostatistics/kxq083.

Thomson EM. 2013. Neurobehavioral and metabolic impacts of inhaled pollutants. Endocr Disruptors (Austin) 1(1):e27489, https://doi.org/10.4161/endo.27489.

van Ewijk H, Heslenfeld DJ, Zwiers MP, Buitelaar JK, Oosterlaan J. 2012. Diffusion tensor imaging in attention deficit/hyperactivity disorder: a systematic review and meta-analysis. Neurosci Biobehav Rev 36(4):1093–1106, PMID: 22305957, https://doi.org/10.1016/j.neubiorev.2012.01.003.

van Tilborg E, de Theije CGM, van Hal M, Wagenaar N, de Vries LS, Benders MJ, et al. 2018. Origin and dynamics of oligodendrocytes in the developing brain: implications for perinatal white matter injury. Glia 66(2):221–238, PMID: 29134703, https://doi.org/10.1002/glia.23256.

Viana M, Kuhlbusch TAJ, Querol X, Alastuey A, Harrison RM, Hopke PK, et al. 2008. Source apportionment of particulate matter in Europe: a review of methods and results. J Aerosol Sci 39(10):827–849, https://doi.org/10.1016/j.jaerosci.2008.05.007.

Weisskopf MG, Seals RM, Webster TF. 2018. Bias amplification in epidemiologic analysis of exposure to mixtures. Environ Health Perspect 126(4):47003, PMID: 29624292, https://doi.org/10.1289/EHP2450.

Weisskopf MG, Sparrow D, Hu H, Power MC. 2015. Biased exposure–health effect estimates from selection in cohort studies: are environmental studies at particular risk? Environ Health Perspect 123(11):1113–1122, PMID: 25956004, https://doi.org/10.1289/ehp.1408888.

Weuve J, Tchetgen EJ, Glymour MM, Beck TL, Aggarwal NT, Wilson RS, et al. 2012. Accounting for bias due to selective attrition: the example of smoking and cognitive decline. Epidemiology 23(1):119–128, PMID: 21989136, https://doi.org/10.1097/EDE.0b013e318230e861.

White T, Muetzel RL, El Marroun H, Blanken LME, Jansen P, Bolhuis K, et al. 2018. Paediatric population neuroimaging and the Generation R Study: the second wave. Eur J Epidemiol 33(1):99–125, PMID: 29064008, https://doi.org/10.1007/s10654-017-0319-y.

White T, Nelson M, Lim KO. 2008. Diffusion tensor imaging in psychiatric disorders. Top Magn Reson Imaging 19(2):97–109, PMID: 19363432, https://doi.org/10.1097/RMR.0b013e3181809f1e.

Yang A, Wang M, Eeftens M, Beelen R, Dons E, Leseman DLAC, et al. 2015. Spatial variation and land use regression modeling of the oxidative potential of fine particles. Environ Health Perspect 123(11):1187–1192, PMID: 25840153, https://doi.org/10.1289/ehp.1408916.